Many-body theory of atomic deuterium

C. W. Greeff,* B. E. Clements,† and E. F. Talbot
Department of Physics, University of Delaware, Newark, Delaware 19711

H. R. Glyde
Department of Physics, University of Alberta, Edmonton, Alberta, Canada T6G 2J1
(Received 10 August 1990)

Deuterium atoms form a fascinating spin-one Fermi fluid of moderate density. Several properties of this fluid are evaluated using the self-consistent Green-function method of many-body theory. The aim is both to determine the properties and to see how well Green-function methods can be implemented in a moderately dense Fermi liquid. Approximations begin with the self-energy. This is separated into Brueckner-Hartree-Fock terms and correlation or two-hole–one-particle (HHP) terms. We find ground-state energies E in reasonable agreement with Monte Carlo values. While the HHP terms are not so important for E, they lead to a significant enhancement of the effective mass m^* at the Fermi surface ε_F. The particle-hole interaction is calculated from the self-energy using the conserving Baym-Kadanoff method. This leads to Landau parameters F_0^s that are positive and an F_1^s that is consistent with m^*.

I. INTRODUCTION

A key purpose of this paper is to test how well properties of a moderately dense Fermi liquid such as atomic deuterium may be evaluated using Green-function methods. The Green-function method we employ is set out in several standard texts on many-body theory.[1–7] We implement the method to evaluate the ground-state energy, single-particle properties such as particle energies, lifetimes, and effective mass, and the interaction appearing in the dynamic susceptibility. We test the results using internal consistency such as the Hugenholtz–van Hove theorem, the equality of effective mass calculated in different ways and by comparison with Monte Carlo (MC) and correlated basis function (CBF) calculations.

The present work is similar in spirit to that of Mahaux and collaborators[6–11] and of Dickoff, Polls, and Ramos[12–15] in nuclear matter. Particularly, we emphasize the role of two-hole–one-particle (HHP) or correlation terms in the self-energy and the consistent treatment of particle and hole propagation.

The deuterium atom consists of a single electron and a deuteron nucleus having nuclear spin $I=1$. The deuterium atom is a composite fermion.[16] We assume the electron spin of each atom is aligned (downward) as if antiparallel to a strong applied field ($D^{\downarrow}$). Only the nuclear spin is a free variable providing a spin $I=1$ Fermi fluid. With electron spins aligned, two $D^{\downarrow}$ atoms interact via the weak $b\,^3\Sigma_u^+$ potential[17] which has a well depth of $\varepsilon\sim 6.4$ K at separation $r_0=4.2$ Å and a core radius $\sigma\approx 3.69$ Å. The $D^{\downarrow}$-$D^{\downarrow}$ potential is compared with the He-He potential for which $\sigma\approx 2.6$ Å in Fig. 1. The saturation volume of liquid deuterium is $V_s\approx 190$ cm^3/mol compared with $V_s\approx 36.8$ cm^3/mol for liquid ^{3}He. Thus, the saturation density $n_s\sigma^3\approx 0.20$ of $D^{\downarrow}$ is approximately one-half that of liquid ^{3}He and atomic deuterium forms a moderately dense Fermi fluid.

Also, with nuclear spin $I=1$, there are three possible spin states, $I_z=1, 0, -1$. We consider models in which all three nuclear spin states are equally occupied ($D_3^{\downarrow}$), two spin states are equally populated ($D_2^{\downarrow}$) and one ($D_1^{\downarrow}$) spin state is populated. This greater spin flexibility allows us to test the role of spin fluctuations more fully than in liquid ^{3}He. A second purpose here is to evaluate the properties of $D^{\downarrow}$.

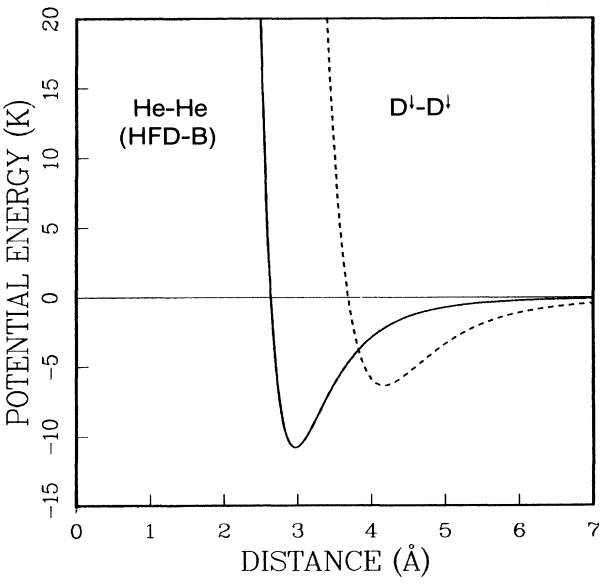

FIG. 1. The $D^{\downarrow}$-$D^{\downarrow}$ potential given by Eq. (1) and the He-He potential (HFD-B of Ref. 44).

In Sec. II we sketch what is known about $D^{\downarrow}$. In Sec. III we outline the Green-function method used here. The spin dependence of the interaction, especially when three nuclear spin states are equally occupied ($D_3^{\downarrow}$), is set out in Sec. IV. The starting point is the first-order self-energy using a T-matrix interaction. Results for the single-particle energies, the effective mass, the ground-state energy, the particle-hole interaction derived from the self-energy using the Baym-Kadanoff[18] method, and Landau parameters are presented in Sec. V. The results are discussed in Sec. VI.

II. ATOMIC DEUTERIUM

To date, atomic deuterium, $D^{\downarrow}$ has been prepared[19] in a high magnetic field B up to densities $n \approx 10^{14}$ atoms/cm^3 only. Early theoretical studies[20–25] showed that $D^{\downarrow}$ formed a highly quantum gas, due to its light mass and relatively weak interaction. At higher densities $D^{\downarrow}$ displays many interesting properties.[20,26–35] MC calculations[27,35] have shown that ($D_2^{\downarrow}$) and ($D_3^{\downarrow}$) form a self-bound liquid when compressed to densities $n \approx 4\times 10^{21}$ atoms/cm^3. The total energy of ($D_1^{\downarrow}$) also has a minimum but the energy is always positive. Superfluidity in $D^{\downarrow}$ has been proposed[29,30] and a Fermi-liquid theory for spin $I=1$ has been developed.[32]

As a model, we assume atomic deuterium (electron spin alignment) but take the applied field $B=0$. We also ignore the hyperfine interaction between electron and nuclear spins. The Hamiltonian is then

$$H=\sum_i^N \frac{p_i^2}{2m}+\sum_{i<j}^N v(r_{ij}) .$$

The pair potential $v(r)$, the same for atomic $H^{\downarrow}$, $D^{\downarrow}$, and $T^{\downarrow}$, has been calculated by Kolos and Wolniewicz[17] for separations $0.5 \le r \le 6.5$ Å. The long-range van der Waals attraction has been evaluated by Bell[36] and by Hirschfelder and Meath.[37] We use Silvera's fit[38] to $v(r)$ as quoted by Friend and Etters,[39]

$$\begin{aligned} V(r)=&\exp(0.096\,78-1.101\,73r-0.3945r^2) \\ &-\{\Theta(r-r_c)-\Theta(r_c-r)\exp[-(r_c/r-1)^2]\} \\ &\times\left[\frac{6.5}{r^6}+\frac{124}{r^8}+\frac{3285}{r^{10}}\right] , \end{aligned} \tag{1}$$

where Θ is the Heaviside step function and $r_c=10.0378$. The r and $v(r)$ are in atomic units.

As noted, with $I=1$, three nuclear spin states $I_z=1$, 0, -1 are possible for each atom. We consider doubly spin polarized D ($D_1^{\downarrow}$) in which only one nuclear spin state is allowed (say, $I_z=-1$), and $D_2^{\downarrow}$ and $D_3^{\downarrow}$ in which two and three spin states are assumed to be equally populated, respectively. As a model, $D_1^{\downarrow}$ is analogous to nuclear spin-polarized ^{3}He (^{3}He$^{\uparrow}$). $D_2^{\downarrow}$ is analogous to normal ^{3}He in which two-spin states are equally populated while $D_3^{\downarrow}$ is a new three-spin-state Fermi fluid. In practice, via the hyperfine interaction, $D^{\downarrow}$ atoms having electron and nuclear spin opposite can flip electron spins which leads to D_2 molecule formation. This removes nuclear spin $\ddagger$ atoms and leaves predominantly nuclear spin-down ($\ddagger$) $D^{\downarrow}$ atoms.[40] Thus, the $D_1^{\downarrow}$ states is most likely to be observed, in practice, providing doubly spin-polarized deuterium. This nuclear spin alignment may be of practical importance in DT fusion reactions.[41]

III. MANY-BODY THEORY

A. Galitskii-Feynman-Hartree-Fock approximation

Our goal is to explore how well properties of the moderately dense fluid, atomic deuterium, can be calculated using Green-function methods beginning from the pair interatomic potential $v(r)$. We begin with approximations to the energy of a single particle in the fluid,

$$\varepsilon_\lambda(p,\omega)=\frac{p^2}{2m}+\Sigma_\lambda(p,\omega) . \tag{2}$$

Here p, ω, and λ are the momentum, energy, and spin of the particle, respectively. For the self-energy we use the lowest-order value, which we call the Galitskii-Feynman-Hartree-Fock (GFHF) approximations,[42]

$$\Sigma_1(1)=-i\int d\bar{2}\sum_2 \Gamma_{1212}(12,12)G_2(2) . \tag{3}$$

Here $1=p_1\omega_1$, the subscripts are nuclear spin labels, and

$$\int d\bar{2}=\int\frac{d^3p_2}{(2\pi)^3}\int\frac{d\omega_2}{2\pi} .$$

The interaction $\Gamma_{1212}(12,12)$ is the diagonal component of the spin-symmetrized interaction

$$\Gamma_{1234}(12,34)=\Gamma(12,34)\delta_{13}\delta_{24}-\Gamma(12,43)\delta_{14}\delta_{23} , \tag{4}$$

which is the sum of a direct [$\Gamma^D=\Gamma(12,34)$] and an exchange [$\Gamma^E=\Gamma(12,43)$] term. The self-energy (3) is derived in standard texts[5] by summing the "ladder" diagrams. In this summation the Fourier transform of the bare potential $v(q)$ is replaced by the T matrix Γ related to $v(q)$ by

$$\begin{aligned} \Gamma(1234)=&v(\mathbf{p}_1-\mathbf{p}_3) \\ &+i\int d\bar{5}v(\mathbf{p}_1-\mathbf{p}_5)G_1(5)G_2(6)\Gamma(56,34) \end{aligned} \tag{5}$$

with a similar equation for Γ^E with indices 3 and 4 interchanged. We call this the Galitskii-Feynman T matrix.[43] By using (4), both the Hartree (Γ^D) and Fock (Γ^E) terms are included in (3). The GFHF self-energy (3) and the GF T matrix (5) are depicted graphically in Fig. 2. The bare potential $v(r)$ enters the theory via (5).

For $G_2(2)$ in (3) and $G_1(5)$ and $G_2(6)$ in (5), we assume the free-particle form

$$\begin{aligned} G(p,\omega)=&\frac{(1-n_p)}{\omega-\varepsilon_p+i\eta}+\frac{n_p}{\omega-\varepsilon_p-i\eta} \\ \equiv&G_P(p,\omega)+G_H(p,\omega) , \end{aligned} \tag{6}$$

where $\varepsilon_p=\varepsilon(p,\varepsilon_p)$ is the "on-energy-shell" value of $\varepsilon(p,\omega)$ in (2). The total $G(p,\omega)$ may be regarded as the sum of particle (P) and hole (H) terms describing propagation of particles above the Fermi sea and holes within

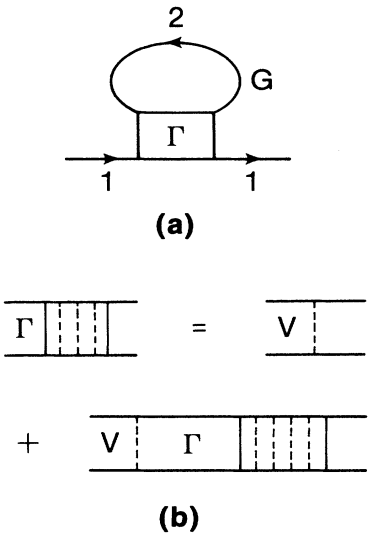

FIG. 2. (a) The lowest-order self-energy, Eq. (3). (b) The Galitskii-Feynman T matrix.

the Fermi sea, respectively. In (6), $n_p=\Theta(\varepsilon_F-\varepsilon_p)$ is the Fermi gas momentum distribution and ε_F is the Fermi energy.

The $\Gamma(12,34)$ is a renormalized interaction between a pair of atoms having initial momentum $\mathbf{p}_1$ and $\mathbf{p}_2$ and total initial energy $E=\omega_1+\omega_2$,

$$\Gamma(12,34)=\Gamma(\mathbf{p}_1\mathbf{p}_2,\mathbf{p}_3\mathbf{p}_4;E=\omega_1+\omega_2)\ . \tag{7}$$

The total energy and momentum are conserved in the interaction,

$$E=\omega_1+\omega_2=\omega_3+\omega_4\ ,$$

$$\mathbf{P}=\mathbf{p}_1+\mathbf{p}_2=\mathbf{p}_3+\mathbf{p}_4\ .$$

Using the form (6) for $G(5)$ and $G(6)$, assuming "on-shell" energies $\varepsilon_5=\varepsilon(p_5,\varepsilon_5)$, and because Γ depends only on E, we may integrate over the energy variable ω_5 in (5) to obtain

$$\begin{aligned}\Gamma(12,34)=&v(\mathbf{p}_1-\mathbf{p}_3)\\&+\int\frac{d^3p_5}{(2\pi)^3}v(\mathbf{p}_1-\mathbf{p}_5)\\&\times\left[\frac{(1-n_5)(1-n_6)}{D+i\varepsilon}-\frac{n_5n_6}{D-i\varepsilon}\right]\\&\times\Gamma(56,34)\ .\end{aligned} \tag{8}$$

Here $D=E-\varepsilon_5-\varepsilon_6$ is the energy denominator. Γ is the sum of a particle-particle (PP) term $(1-n_5)(1-n_6)$ representing scattering to intermediate particle states above the Fermi sea and a hole-hole (HH) term (n_5n_6) representing scattering to intermediate states within the Fermi sea. The form (8) displays the symmetric treatment of particle and hole states in Γ. If only the PP term in (8) is retained, Γ reduces to the Brueckner G matrix. Equation (8) is discussed in detail by Ramos *et al.*[15]

B. Properties of the GFHF approximation

The GFHF approximation consists of iterating the above equations (2)–(4) and (8) until consistent with $E=\varepsilon_1+\varepsilon_2$ set at its "on-energy-shell" value. In general, $\Sigma(p,\omega)$ is complex and we iterate the equation both with and without the imaginary part of $\Sigma(p,\omega)$ for comparison. Once the iteration is complete, "off-energy-shell" values of $\Sigma_\lambda(p,\omega)$ and related properties can be calculated. The GFHF model has several features. A continuous single-particle energy (2) is used with no gap at the Fermi surface.[6,7] There is a symmetric treatment of particle and hole states[12–15] in both G and Γ. In the more usual Brueckner G matrix, scattering to only intermediate particle states is included.

The GFHF self-energy depicted in Fig. 2 can be derived as the lowest-order self-energy, obtained by summing "ladder" diagrams (e.g., p. 85, Ref. 1). However, it is interesting to note that the self-energy which is second order in Γ contains no new diagrams that are not already in the first order Σ, Eq. (3). The second-order self-energy, depicted in Fig. 3(a), is

$$\begin{aligned}&\Sigma^{(2)}(1)\\&=\tfrac{1}{2}\int d\bar{2}\int d\bar{5}\Gamma(15,26)G(5)G(6)\Gamma(62,51)G(2)\ .\end{aligned} \tag{9}$$

Spin indices are omitted in (9). In $\Sigma^{(2)}(1)$, Γ is written in the configuration of a particle-hole interaction. To see that $\Sigma^{(2)}(1)$ contains no topologically different diagrams from (3) when expression in terms of the bare interaction $v(q)$, note that the T matrix in (3) contains terms such as

$$\frac{i}{2}\int d\bar{5}\Gamma(12,56)G(5)G(6)\Gamma(56,12) \tag{10}$$

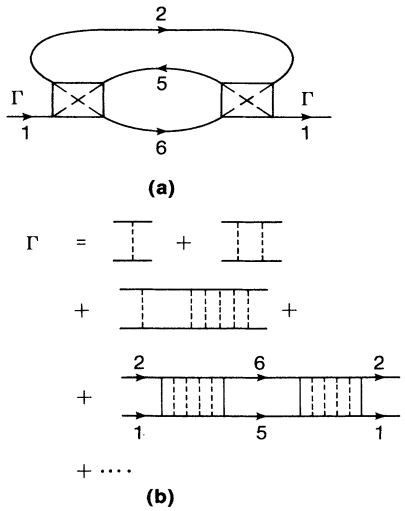

FIG. 3. (a) The second-order self-energy, Eq. (9). (b) Terms contained in the Galitskii-Feynman T matrix.

as depicted in Fig. 3(b). The first-order self-energy in (3) due to this term (10) of Γ is

$$\Sigma(1) = -i\frac{i}{2}\int d\bar{2}\int d\bar{5}\Gamma(12,56)G(5)G(6)\Gamma(56,12)G(2)\ . \tag{11}$$

By formally interchanging the labels 5 and 2 and using $\Gamma(26,15)=\Gamma(62,51)$, we may write (11) as

$$\Sigma(1)=\tfrac{1}{2}\int d\bar{2}\int d\bar{5}\Gamma(15,26)G(5)G(6)\Gamma(62,51)G(2)\ , \tag{12}$$

which is the same as the second-order self-energy (9). Thus, the second-order term (9) is not topologically distinct from the first-order GFHF term.

C. Σ_{PPH} and Σ_{HHP}

To compare with previous studies[15,33,43] and to identify the origin of specific properties, it is convenient to separate Σ into two parts,

$$\Sigma=\Sigma_{PPH}+\Sigma_{HHP} \tag{13}$$

following Ramos *et al.*[12] Here P (H) denotes a particle (hole) contribution to Σ in the spirit of the hole-line expansion, as specified below. In (6), we saw that the Green-function separates naturally into a particle and a hole term. From (8), the T matrix separates into a PP and a HH term. This separation appears generally in the Lehman representation of Γ. Suppressing the momentum indices, this representation is

$$\Gamma(E)=\int_0^\infty\frac{dx}{2\pi}\left[\frac{\Gamma_1(x)}{E-2\mu-x+i\eta}-\frac{\Gamma_2(x)}{E-2\mu+x-i\eta}\right] \equiv\Gamma_{PP}(E)+\Gamma_{HH}(E)\ , \tag{14}$$

where $\mu=\varepsilon_F$. The $\Gamma_{PP}(E)$ has particle poles lying below the real axis at $E=2\mu+x-i\eta$. Substituting (14) and (6) into (3), the self-energy is

$$\begin{aligned}\Sigma(\omega_1)&=-i\int\frac{d^3p_2}{(2\pi)^3}\int\frac{d\omega_2}{(2\pi)}[\Gamma_{PP}(\omega_1+\omega_2)+\Gamma_{HH}(\omega_1+\omega_2)][G_p(\omega_2)+G_H(\omega_2)]\\ &=\int\frac{d^3p_2}{(2\pi)^3}[\Gamma_{PP}(\omega_1+\varepsilon_2)n_2-\Gamma_{HH}(\omega_1+\varepsilon_2)(1-n_2)]\\ &\equiv\tilde{\Sigma}_{PPH}(\omega_1)+\tilde{\Sigma}_{HHP}(\omega_1)\ .\end{aligned} \tag{15}$$

In (15), the integration over ω_2 has been done by contour integration and closing the contour above or below the real axis to avoid the poles in $\Gamma(\omega_1+\omega_2)$. Clearly, $\tilde{\Sigma}_{HHP}$ contains two hole lines from the second term Γ_{HH} in Γ and a particle line $(1-n_2)$. The $\tilde{\Sigma}_{PPH}$ is structurally the same as the usual Brueckner-Hartree-Fock (BHF) self-energy.[7] However, since we retain both terms in (8) for the interaction, Γ, the value may be somewhat different from the BHF value calculated with a G matrix. On the basis of the hole-line expansion, we expect $\tilde{\Sigma}_{HHP}$ to be smaller than $\tilde{\Sigma}_{PPH}$.

Using the analytic properties of Γ in (14), the imaginary part of $\Sigma(p,\omega)$ is

$$\begin{aligned}\Sigma''(p_1,\omega_1)&=\int\frac{d^3p_2}{(2\pi)^3}\Gamma''(\omega_1+\varepsilon_2)\\ &\quad\times[\Theta(\omega_1+\varepsilon_2-2\mu)\Theta(\mu-\varepsilon_2)\\ &\quad-\Theta(2\mu-\omega_1-\varepsilon_2)\Theta(\varepsilon_2-\mu)]\\ &\equiv\tilde{\Sigma}''_{PPH}(\omega_1)+\tilde{\Sigma}''_{HHP}(\omega_1)\ .\end{aligned} \tag{16}$$

The first term Σ''_{PPH} clearly contributes for $\omega_1>\mu$ only while the second term Σ''_{HHP} contributes for $\omega_1<\mu$ only. Using

$$\Theta(x-2\mu)=1-\Theta(2\mu-x)\ ,$$

Σ'' can be written as

$$\Sigma''(p_1,\omega_1)=\int\frac{d^3p_2}{(2\pi)^3}\Gamma''(\omega_1+\varepsilon_2)\times[\Theta(\mu-\varepsilon_2)-\Theta(2\mu-\omega_1-\varepsilon_2)]\ , \tag{17}$$

which is the form we evaluated. From (17) it is clear that $\Sigma''(p_1,\omega_1)$ must vanish at $\omega_1=\mu$.

Combining terms in (15) and using the analytic properties of Γ in (14), the real part of $\Sigma(p,\omega)$ may be written as

$$\begin{aligned}\Sigma'(p_1,\omega_1)&=\int\frac{d^3p_2}{(2\pi)^3}[\Gamma'(\omega_1+\omega_2)n_2-\Gamma'_{HH}(\omega_1+\varepsilon_2)]\\ &=\int\frac{d^3p_2}{(2\pi)^3}\left[\Gamma'(\omega_1+\omega_2)n_2-\mathrm{P}\int_{-\infty}^{2\mu}\frac{dy}{\pi}\frac{\Gamma''(y)}{\omega_1+\varepsilon_2-y}\right]\\ &\equiv\Sigma'_{PPH}(p_1,\omega_1)+\Sigma'_{HHP}(p_1,\omega_1)\ .\end{aligned} \tag{18}$$

The Σ'_{PPH} is $\tilde{\Sigma}'_{PPH}$ but including the HH terms in Γ to complete Γ. Thus, strictly Σ'_{PPH} contains both the PP and HH lines in Γ. From previous work, scattering to particle states dominates Γ. Similarly, $\Sigma'_{HHP}(p_1,\omega_1)$ contains both particle and hole states in G.

Because $\tilde{\Sigma}''_{PPH}(p,\omega)$ contributes only for $\omega>\mu$ and $\tilde{\Sigma}''_{HHP}(p,\omega)$ contributes only for $\omega<\mu$, the corresponding real parts are often denoted as the polarization potential

$[V_{\rm po}=\tilde{\Sigma}'_{\rm PPH}(p,\omega)]$ and correlation potential $[V_{\rm co}=\tilde{\Sigma}'_{\rm HHP}(p,\omega)]$, respectively. The $V_{\rm po}$ is clearly the Brueckner-Hartree-Fock potential. The $V_{\rm co}$ is also denoted as the rearrangement energy. In previous work, we evaluated the full $\Sigma''(p,\omega)$ in (17) including both $\tilde{\Sigma}''_{\rm PPH}$ and $\tilde{\Sigma}''_{\rm HHP}$. However, we evaluated only $\Sigma'_{\rm PPH}$ in the real part. A chief goal here is to include $\Sigma'_{\rm HHP}$ and investigate its size and character. The $\Sigma'_{\rm HHP}$ has been included in nuclear matter by Ramos *et al.*[12–15] and as an addition to the Brueckner-Hartree-Fock by Mahaux *et al.*[9–11]

IV. SPIN DEPENDENCE OF THE INTERACTION

In this section we set out the spin dependence of the interaction $\Gamma_{1234}(12,34)$ in (4) for $D_1^{\downarrow}$, $D_2^{\downarrow}$, and $D_3^{\downarrow}$.

A. $D_1^{\downarrow}$

In $D_1^{\downarrow}$, with all nuclear spins aligned, there is only a single interaction $\Gamma_{\uparrow\uparrow\uparrow\uparrow}$. If we introduce relative incoming and outgoing momenta, $\mathbf{k}=\frac{1}{2}(\mathbf{p}_1-\mathbf{p}_2)$ and $\mathbf{k}'=\frac{1}{2}(\mathbf{p}_3-\mathbf{p}_4)$, respectively, and the usual angle averaging over the c.m. momentum P, we may expand Γ^D in (4) in angular-momentum components

$$\Gamma^D(\mathbf{k},\mathbf{k}',\mathbf{P})=\sum_L(2L+1)\Gamma_L P_L(\cos\Theta_{kk'}) \ . \tag{19}$$

Expanding both the diagonal Γ^D and Γ^E in (4) using (19), we find $\Gamma_{\uparrow\uparrow\uparrow\uparrow}$ contains only odd-angular-momentum components

$$\Gamma^S\equiv\Gamma_{\uparrow\uparrow\uparrow\uparrow}=\Gamma^D(\mathbf{k},\mathbf{k},\mathbf{P})-\Gamma^E(\mathbf{k},-\mathbf{k},\mathbf{P})=2a_0 \ , \tag{20}$$

where

$$a_0=\sum_{\substack{L\\ \text{odd}}}(2L+1)\Gamma_L(k,P) \tag{21}$$

is a sum over odd-L components of Γ_L. Equivalently, since the spin state is symmetric, the space state is antisymmetric and $\Gamma_{\uparrow\uparrow\uparrow\uparrow}$ contains only odd-angular-momentum components. We evaluated Γ^S by evaluating the individual Γ_L and summing.

B. $D_2^{\downarrow}$

$D_2^{\downarrow}$ has two equally populated spin states as in a spin-$\frac{1}{2}$ Fermi liquid (e.g., normal ^{3}He). As in liquid ^{3}He, the spin-symmetric and spin-antisymmetric interactions are

$$\begin{aligned}\Gamma^s&=\tfrac{1}{2}(\Gamma_{\uparrow\uparrow\uparrow\uparrow}+\Gamma_{\uparrow\downarrow\uparrow\downarrow})=\tfrac{1}{2}(3a_0+a_e) \ ,\\ \Gamma^a&=\tfrac{1}{2}(\Gamma_{\uparrow\uparrow\uparrow\uparrow}-\Gamma_{\uparrow\downarrow\uparrow\downarrow})=\tfrac{1}{2}(a_0-a_e) \ .\end{aligned} \tag{22}$$

C. $D_3^{\downarrow}$

In this case we have fermions of nuclear spin $I_i=1$, in which the three-spin states $I_{iz}=-1,0,1$ are equally populated. Since we take $B=0$ and there are no explicitly spin-dependent forces, the spin dependence of the interaction is introduced by the symmetry imposed on the space state by the symmetry of the spin state. The interaction in a space-symmetric state involves only the even-l components of Γ $(2a_e)$ and a space-antisymmetric state involves the odd-l components $(2a_0)$.

Note that the operator

$$\mathbf{I}_i\cdot\mathbf{I}_j+(\mathbf{I}_i\cdot\mathbf{I}_j)^2=2P_s \ ,$$

where P_s is the projection operator on spin-symmetric states; that is,

$$\begin{aligned}P_s|I=2\rangle&=|I=2\rangle \ ,\\ P_s|I=1\rangle&=0 \ ,\\ P_s|I=0\rangle&=|I=0\rangle \ ,\end{aligned}$$

where $I=I_i+I_j$ is the total spin and $I=0,2$ are the spin-symmetric states and $I=1$ is the spin-antisymmetric state. Then, the general form for the spin dependence of the interaction is

$$\Gamma_{1234}=\Gamma_1\delta_{13}\delta_{24}+\Gamma_2\langle 12|(\mathbf{I}_i\cdot\mathbf{I}_j)+(\mathbf{I}_i\cdot\mathbf{I}_j)^2|34\rangle \ . \tag{23}$$

Then one easily obtains

$$\begin{aligned}\Gamma^{I=2}_{\uparrow\uparrow\uparrow\uparrow}&=\Gamma_1+2\Gamma_2=2a_0 \ ,\\ \Gamma^{I=1}&=\Gamma_1=2a_e \ ,\end{aligned} \tag{24}$$

which gives

$$\begin{aligned}\Gamma_1&=2a_e \ ,\\ \Gamma_2&=a_0-a_e \ .\end{aligned} \tag{25}$$

This allows us to express Γ_{1234} in terms of the Γ_L in (23). The three nonvanishing interactions are

$$\begin{aligned}\Gamma_{\uparrow\uparrow\uparrow\uparrow}&=\Gamma_{\rightarrow\rightarrow\rightarrow\rightarrow}=\Gamma_1+2\Gamma_2 \ ,\\ \Gamma_{\uparrow\downarrow\uparrow\downarrow}&=\Gamma_{\uparrow\rightarrow\uparrow\rightarrow}=\Gamma_1+\Gamma_2 \ ,\\ \Gamma_{\uparrow\downarrow\downarrow\uparrow}&=\Gamma_{\rightarrow\uparrow\uparrow\rightarrow}=\Gamma_2 \ .\end{aligned} \tag{26}$$

For $I_i=1$, the spin-symmetric interaction which appears in density-dependent properties and the spin-antisymmetric interaction which appears in magnetic properties are conveniently defined as

$$\begin{aligned}\Gamma^s&=\tfrac{1}{3}\Gamma_{\uparrow\uparrow\uparrow\uparrow}+(\Gamma_{\uparrow\rightarrow\uparrow\rightarrow}+\Gamma_{\uparrow\downarrow\uparrow\downarrow})=\tfrac{1}{3}(4a_0+2a_e) \ ,\\ \Gamma^a&=\tfrac{1}{3}(\Gamma_{\uparrow\uparrow\uparrow\uparrow}-\Gamma_{\uparrow\downarrow\uparrow\downarrow})=\tfrac{1}{3}(a_0-a_e) \ .\end{aligned} \tag{27}$$

The $\Gamma_{\uparrow\rightarrow\uparrow\rightarrow}$ does not appear in Γ^a because spins perpendicular to the z axis $(\rightarrow)$ do not contribute to the magnetization. Using (27) we can relate Γ^s and Γ^a to the calculated Γ_L.

V. RESULTS

In this section we present results for the single-particle energies $\varepsilon(k)$, the effective mass $m^*(k)$, the ground-state energy E, and the particle-hole interaction $I_{p\text{-}h}$, within the GFHF approximation in Sec. V A–V D, respectively.

A. Single-particle energies

The GFHF single-particle energies are given by Eqs. (2) and (3). From (2) and (18), the real part of the on-energy-shell single-particle energy is

$$\begin{aligned}\mathrm{Re}\varepsilon(k) &= \mathrm{Re}\varepsilon(k,\varepsilon(k)) \\ &= \varepsilon^0(k) + N_s \int \frac{d^3p_2}{(2\pi)^3} \left[\Gamma^{s'}(12;\varepsilon_1+\varepsilon_2)n_2 - \mathrm{P}\int_{-\infty}^{2\mu} (dy/\pi) \frac{\Gamma^{s''}(12;y)}{\varepsilon_1+\varepsilon_2-y} \right] \\ &\equiv \varepsilon^0(k) + \Sigma'_{\mathrm{PPH}}(k) + \Sigma'_{\mathrm{HHP}}(k) \ . \end{aligned} \tag{28}$$

Here $\varepsilon^0(k)=(\hbar k)^2/2m$, $\Gamma^s(12,\varepsilon_1+\varepsilon_2)$ is the diagonal and on-energy-shell T matrix (8) and $\varepsilon_1=\varepsilon(k_1)$. The Γ^s is the spin-symmetric value of the T matrix defined in Sec. IV and N_s is the number of spin states; $N_s=1$, 2, and 3 in D_1, D_2, and D_3, respectively. The imaginary part of $\varepsilon(k)$ is given by the on-energy-shell value of (17). Summation over the spin states in (17) also leads to the interaction $N_s\Gamma^{s''}$.

In Figs. 4–6 we show the $\varepsilon(k)$ for D_1, D_2, and D_3. These were obtained by iterating Eqs. (2), (3), and (8) retaining only the real part of $\varepsilon(k)$ in the T matrix during iteration. The imaginary part of $\varepsilon(k)$ in Figs. 4–6 was calculated using the converged T matrix. In Fig. 4 we see that $\mathrm{Re}\varepsilon(k)$ for D_1 moves to lower energy as the density n is increased. Here $n_s \simeq 3.5\times10^{-3}$ Å^{-3} is the saturation density. However, the shape of $\mathrm{Re}\varepsilon(k)$ in Fig. 4 is largely independent of density. The $\mathrm{Im}\varepsilon(k)$ is positive for $k<k_F$ due to $\tilde{\Sigma}''_{\mathrm{HHP}}$ and negative for $k>k_F$ due to $\tilde{\Sigma}''_{\mathrm{PPH}}$.

In Fig. 5 for $D_2^{\downarrow}$ we see that $\mathrm{Re}\varepsilon(k)$ shows a flattening at $k\approx k_F$. The magnitude of this flattening increases with increasing density. In Fig. 6 for $D_3^{\downarrow}$ we see a similar and more pronounced flattening of $\mathrm{Re}\varepsilon(k)$ at $k\simeq k_F$, especially at high density. Also, substantial structure appears in $\varepsilon(k)$ for $D_2^{\downarrow}$ and $D_3^{\downarrow}$ at $k<k_F$ at higher density.

The flattening of $\varepsilon(k)$ at $k\approx k_F$ and the structure in $\varepsilon(k)$ have the following origins. Firstly, the flattening of $\mathrm{Re}\varepsilon(k)$ at $k=k_F$ comes predominantly from Σ'_{HHP}, the correlation potential. In the lower half of Fig. 7 we show $\mathrm{Re}\varepsilon(k)$ with (line 1) and without (line 2) Σ'_{HHP}. Clearly, including only Σ'_{PPH} line 2 in Fig. 7, we obtain a nearly parabolic $\varepsilon(k)$. $\Sigma'_{\mathrm{PPH}}(k)$ and $\Sigma'_{\mathrm{HHP}}(k)$ are shown in the upper half of Fig. 7. $\Sigma'_{\mathrm{HHP}}(k)$ makes a positive or "unbinding" contribution to $\varepsilon(k)$ for $k>0.2$ Å^{-1}. The magnitude of $\Sigma'_{\mathrm{HHP}}(k)$ from Fig. 7 clearly reaches a maximum below k_F and falls rapidly near k_F. This drop in Σ'_{HHP} leads to a flattening in $\varepsilon(k)$.

The flattening of $\varepsilon(k)$ at k_F also apparently depends on spin fluctuations. There is no flattening of $\mathrm{Re}\varepsilon(k)$ in $D_1^{\downarrow}$ where all spins are aligned and spin fluctuations are frozen out. The flattening is more pronounced in $D_3^{\downarrow}$ than in $D_2^{\downarrow}$. In $D_3^{\downarrow}$ where three spin states are allowed, spin fluctuations may be expected to play a larger role.

In general, we found that the iteration between the T matrix and $\varepsilon(k)$ converged most rapidly and to the most stable solution at low density for $D_1^{\downarrow}$. This might be ex-

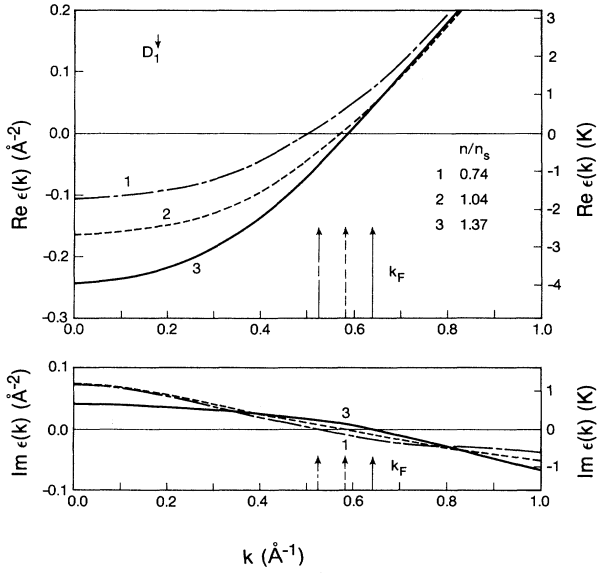

FIG. 4. The real and imaginary part of the single-particle energy $\varepsilon(k)$ given by Eqs. (28) and (17), respectively, in $D_1^{\downarrow}$ at three densities n. The $n_s=3.35\times10^{21}$ atoms/cm^3. Only the $\mathrm{Re}\varepsilon(k)$ was retained in the iterations and $\mathrm{Im}\varepsilon(k)$ was evaluated afterward.

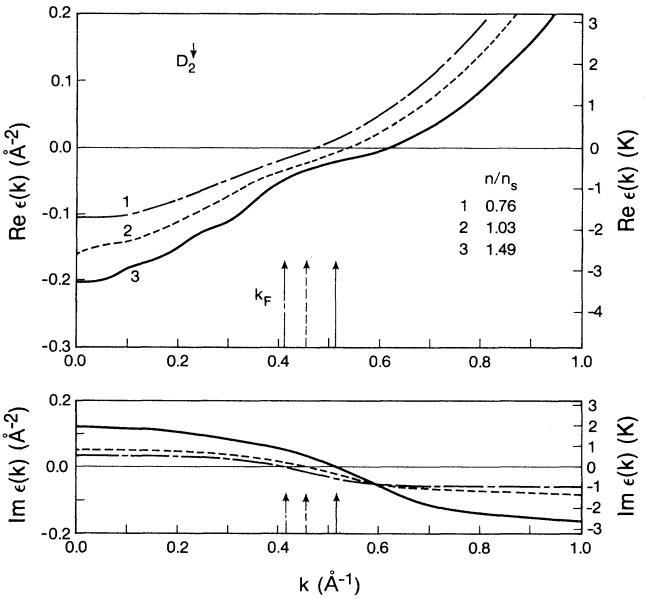

FIG. 5. The same as Fig. 4 for $D_2^{\downarrow}$; $n_s=3.17\times10^{21}$ atoms/cm^3.

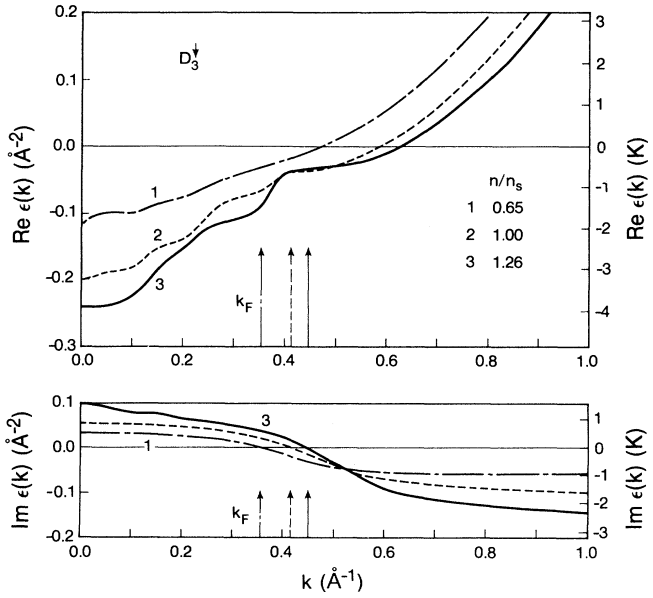

FIG. 6. The same as Fig. 4 for $D_3^{\downarrow}$; $n_s = 3.54 \times 10^{21}$ atoms/cm^3.

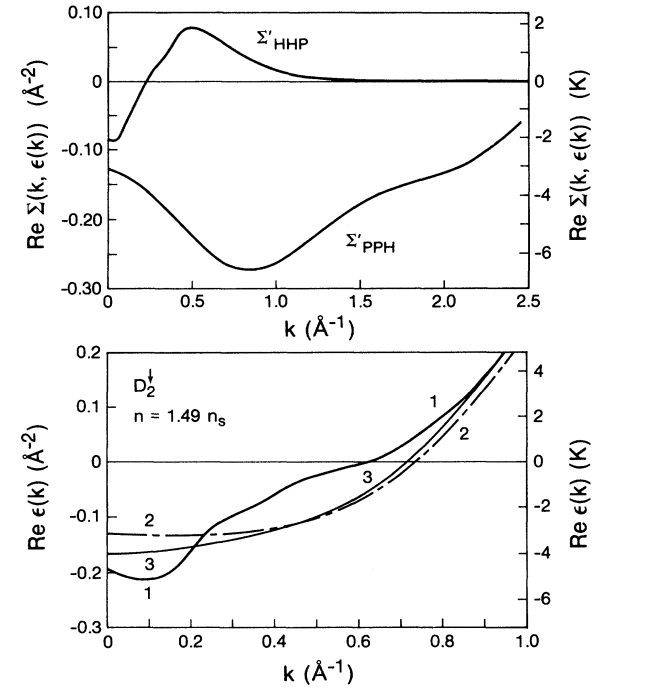

FIG. 7. Upper: Final iterated values of Σ'_{PPH} and Σ'_{HHP}, given by Eq. (18), in $D_2^{\downarrow}$ at density $n = 1.49 n_s$. Lower: Line 1 is the corresponding self-consistent value of $\varepsilon(k) = \varepsilon^0(k) + \Sigma'_{PPH} + \Sigma'_{HHP}$, line 3 is $\varepsilon(k) = \varepsilon^0(k) + \Sigma'_{PPH}$ (line 1 without Σ'_{HHP}), and line 2 is the self-consistent $\varepsilon(k) = \varepsilon^0(k) + \Sigma'_{PPH}$ obtained by iterating with Σ'_{PPH} only.

pected since the present many-body theory is a low-density theory. Also, in $D_1^{\downarrow}$ the exchange interaction operates between all spins. This exchange correlation is included in the GFHF self-energy and provides correlations between all particles in $D_1^{\downarrow}$. The exchange correlations in $D_1^{\downarrow}$ reduce the need for an explicit description of higher-order correlations so that GFHF is a better theory for $D_1^{\downarrow}$ than for $D_2^{\downarrow}$ or $D_3^{\downarrow}$.

Convergence of the iteration was slowest and least stable for $D_2^{\downarrow}$ and $D_3^{\downarrow}$ at high density. In Fig. 8 we show $\mathrm{Re}\varepsilon(k)$ obtained in the last few iterations for D_2 at $n = 1.03 n_s$ and $n = 1.47 n_s$. At $n \approx n_s$, the final few $\mathrm{Re}\varepsilon(k)$ all lie on a single line except at $k \approx 0$. At $n \approx 1.5 n_s$, the $\mathrm{Re}\varepsilon(k)$ does not converge well at all for $k \leq 0.3$ Å^{-1}. However, the flattening of $\varepsilon(k)$ at $k \approx k_F$ appears in all the final few $\varepsilon(k)$ so that we believe this flattening is well determined. The structure in $\varepsilon(k)$ at low k ($k \leq 0.3$ Å^{-1}) is not well determined. We believe the poor convergence at higher density in $D_2^{\downarrow}$ and $D_3^{\downarrow}$ is due to the nonmonatomic behavior of $\varepsilon(k)$ introduced by Σ'_{HHP} which we were not able to describe well from one iteration to the next.

Convergence was rapid and stable when only Σ'_{PPH}, the Brueckner-Hartree-Fock potential, was included. This was especially true when the full complex $\varepsilon(k)$ was included in the iteration. In all cases when $\varepsilon''(k)$ was included in the iteration, we retained the full imaginary part, Σ''_{PPH} and Σ''_{HHP}. The converged $\mathrm{Re}\varepsilon(k)$ had somewhat lower energy when $\varepsilon''(k)$ was included in the iteration, leading to a somewhat lower ground-state energy, as discussed in Sec. III C.

B. Effective mass

The effective mass is defined as

$$m^*(k) = k \left[\frac{d\varepsilon(k)}{dk} \right]^{-1} . \tag{29}$$

This is a total derivative of the on-energy-shell $\varepsilon(k)$ in which all components entering $\varepsilon(k)$ (the single-particle

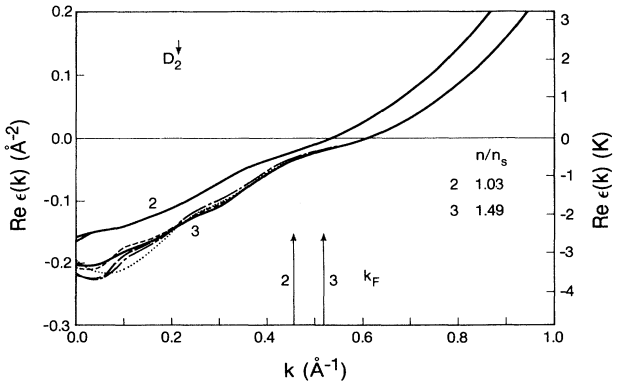

FIG. 8. Values of $\mathrm{Re}\varepsilon(k)$ obtained from the last few iterations in $D_2^{\downarrow}$; at $n = 1.03 n_s$ and $1.49 n_s$.

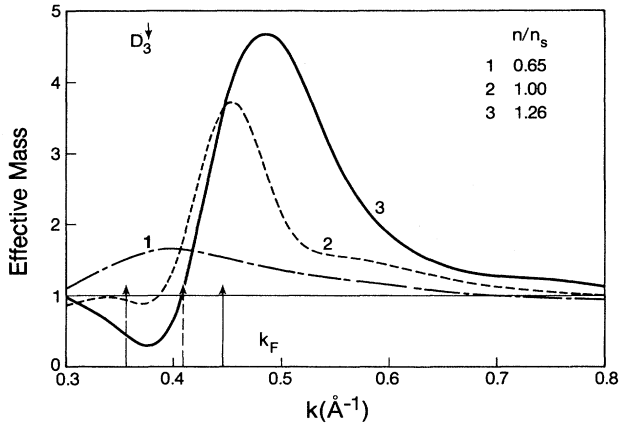

FIG. 9. Effective mass of $D_3^\downarrow$ obtained by differentiating Re$\varepsilon(k)$ of Fig. 6 using Eq. (29) at these densities.

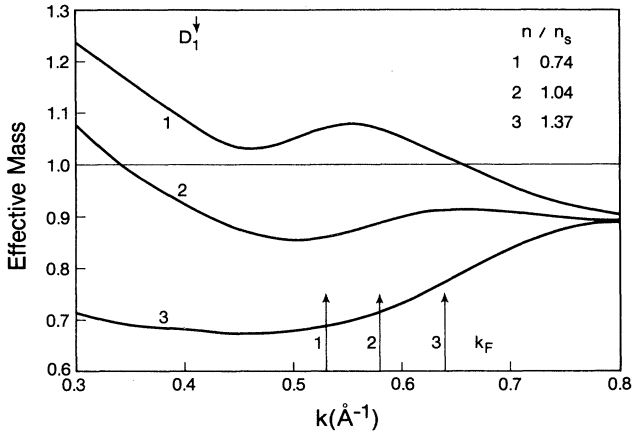

FIG. 11. Effective mass of $D_1^\downarrow$ obtained from Re$\varepsilon(k)$ in Fig. 4.

energies and the T matrix) change with k. We evaluated $m^*(k)$ by numerically differentiating the Re$\varepsilon(k)$ shown in Figs. 4–6.

In Fig. 9 we show $m^*(k)$ for $D_3^\downarrow$ at three densities. The $m^*(k)$ is clearly enhanced well above unity at k values slightly larger than k_F. This mass enhancement follows from the flattening of $\varepsilon(k)$ near k_F and increases with increasing density. In liquid ^{3}He, $m^*(k_F)$ increases from $m^* \approx 3$ to 5 between saturated vapor pressure (SVP) and $p=25$ bars. Clearly when spin fluctuations are possible, $m^*(k)$ can show enhancement in $D^\downarrow$. An enhancement of $m^*(k)$ near k_F was apparently first proposed by Brown *et al.*[45] for nuclei. The present calculations suggest this enhancement is due to spin fluctuations and it increases with density as observed in liquid ^{3}He. The $m^*(k)$ shown in Fig. 9 are calculated from an average of (29) over the final few spectra $\varepsilon(k)$ to obtain smooth values.

In Fig. 10 is $m^*(k)$ for $D_2^\downarrow$ at three densities. The $m^*(k)$ again peaks at $k \approx k_F$ and $m^*(k_F)$ increases with increasing density. The magnitude of $m^*(k_F)$ is, however, significantly smaller in $D_2^\downarrow$ than in $D_3^\downarrow$. The $m^*(k)$ for $D_1^\downarrow$ is shown in Fig. 11. In this case there is no effective mass enhancement and $m^*(k)$ appears to decrease with increasing density if anything. We do not attribute any significance to the small peak in $m^*(k)$ at the low density $n=0.74n_s$ in $D_1^\downarrow$.

In Fig. 12 we compare $m^*(k)$ for $D_1^\downarrow$, $D_2^\downarrow$, and $D_3^\downarrow$ at their respective saturation densities. The increasing enhancement of $m^*(k_F)$ with an increasing number of spin states strongly suggests the enhancement is related to spin fluctuations. The width of the peak in $m^*(k)$ is comparable to that found in nuclear matter.[6,7] The enhancement here is due almost entirely to the correlation term $\Sigma'_{\rm HHP}$ which produces the flattening of $\varepsilon(k)$ at $k=k_F$. We have not attempted to separate m^* into its "k mass" and "E mass" components.

In Table I we compare the $m^*(k_F)$ at $k=k_F$ obtained

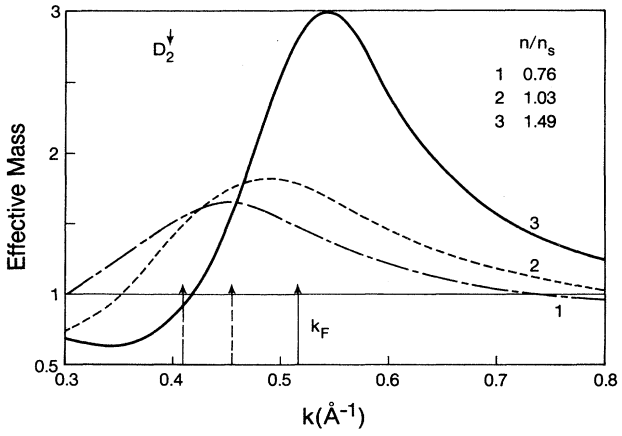

FIG. 10. Effective mass of $D_2^\downarrow$ obtained from Re$\varepsilon(k)$ in Fig. 5.

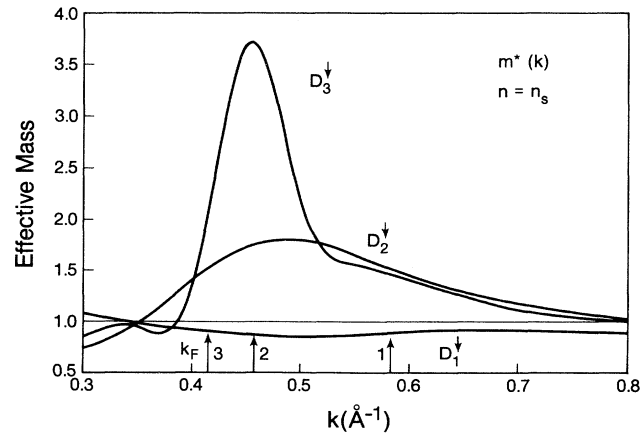

FIG. 12. Effective mass m^* given by Eq. (29) in $D_1^\downarrow$, $D_2^\downarrow$, and $D_3^\downarrow$ at saturation density n_s in each case.

TABLE I. Effective mass calculated from Landau parameters ($m^*=1+F_1^s/3$) and from the $m^*(k_F)=k_F[d\varepsilon(k)/dk]_{k_F}^{-1}$ from Fig. 12.

	$D_1^\downarrow$	$D_2^\downarrow$	$D_3^\downarrow$
$(1+F_1^s/3)$	0.94	1.67	2.43
$m^*(k_F)$	0.90	1.7	2.2–3.0

from (29) with the m^* calculated using the Landau relation $m^*=(1+F_1^s/3)$. In the latter, F_1^s was calculated from the converged T matrix at low wave vector as discussed in Sec. V D. From Table I we see that the m^* calculated by the two independent methods agree well.

C. Ground-state energy

The total energy may be obtained as

$$\frac{E}{N}=\tfrac{3}{5}\varepsilon_F^0+\frac{N_s}{2N}\sum_{k_1}\Sigma'(k_1,\varepsilon_1)n_1\ , \tag{30}$$

where $\Sigma'(k_1,\varepsilon_1)$ is the real part of the on-shell self-energy in (28). In Fig. 13, we show E/N for the nuclear spin-polarized case $D_1^\downarrow$. In Fig. 13, the line marked E is the full GFHF value including $\Sigma'_{\rm PPH}$ and $\Sigma'_{\rm HHP}$ and iterated with real $\varepsilon(k)$. The E'_R is E iterated with real energies $\varepsilon(k)$ but with the correlation term $\Sigma'_{\rm HHP}$ omitted. By comparing E and E'_R, we see that $\Sigma'_{\rm HHP}$ makes a positive contribution to E. The magnitude of $\Sigma'_{\rm HHP}$ increases with density. From the hole-line expansion picture, we expect terms containing hole lines (two in this case) to increase

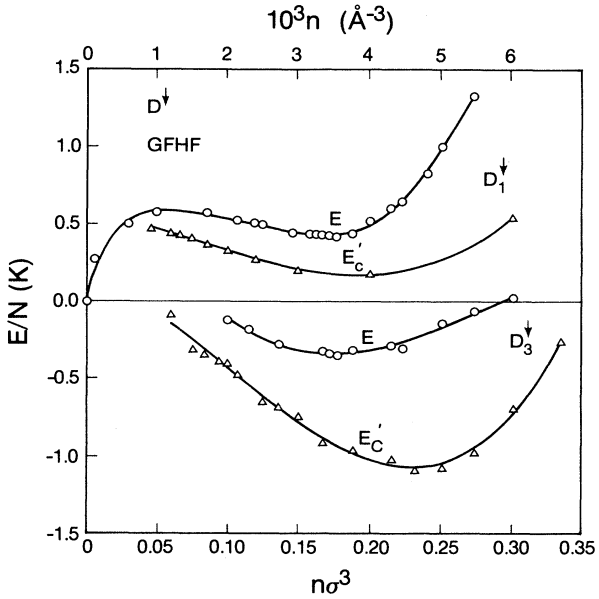

FIG. 14. Ground-state energy of $D_1^\downarrow$ and $D_3^\downarrow$. E is the full GFHF energy iterated using a real $\varepsilon(k)$, and E'_C is the GFHF energy iterated with a complex $\varepsilon(k)$ but without $\mathrm{Re}\Sigma_{\rm HHP}$.

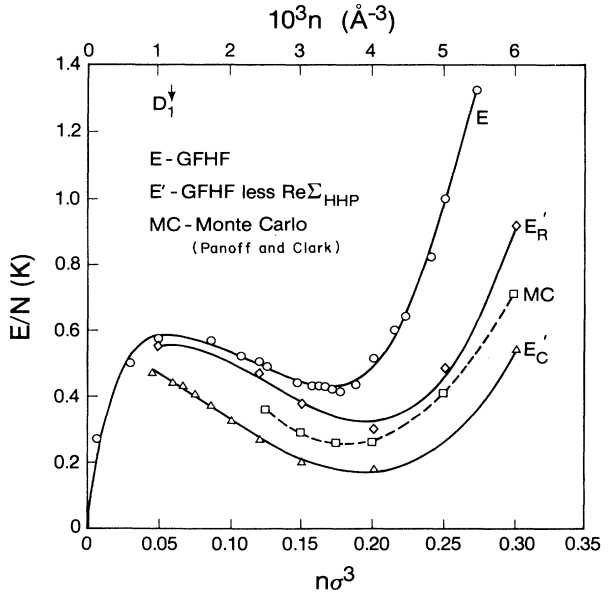

FIG. 13. Ground-state energy of doubly spin-polarized deuterium $D_1^\downarrow(\sigma^3=3.69)$. E is the full Galitskii-Feynman-Hartree-Fock (GFHF) energy iterated using a real single-particle energy spectrum $\varepsilon(k)$, E'_R in the GFHF energy iterated using a real $\varepsilon(k)$ without $\mathrm{Re}\Sigma_{\rm HHP}$, E'_C is the same as E'_R but using a complex $\varepsilon(k)$. MC is the Monte Carlo result $D_1^\downarrow(\sigma^3=3.69)$ of Panoff and Clark (Ref. 34).

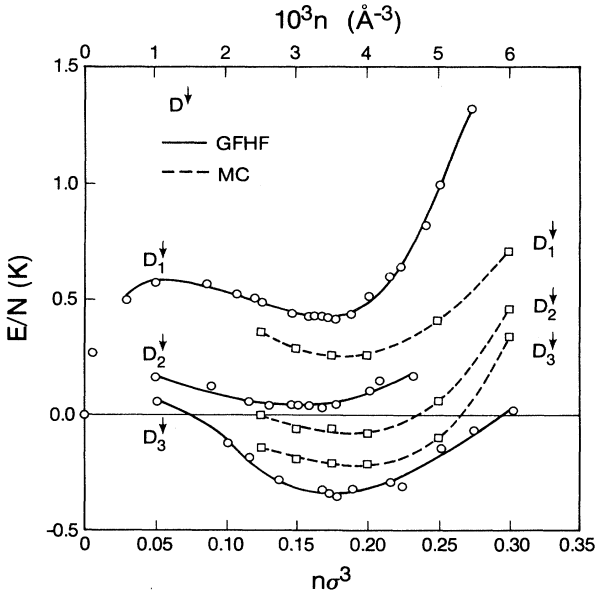

FIG. 15. Ground-state energy of $D_1^\downarrow$, $D_2^\downarrow$, and $D_3^\downarrow$. The solid line is the GFHF energy iterated using a real $\varepsilon(k)$, and the dashed line is the MC values of Panoff and Clark (Ref. 34).

TABLE II. Parameters of Eq. (31) obtained by fitting (31) to the GFHF energy shown in Fig. 15.

	$(10^3 n_s\sigma^3)$	E_s (K)	A (K)	B (K)	C (K)
$D_1^\downarrow$	0.1685	0.454	1.096	1.44	
	0.1633	0.414	1.525	1.11	−0.82
$D_2^\downarrow$	0.1559	0.0291	0.776	0.70	
	0.1541	0.0287	0.773	0.50	−0.30
$D_3^\downarrow$	0.1729	−0.3123	0.930	−0.44	
	0.1724	−0.3123	0.918	−0.48	0.069

as k_F increases. The contribution of $\Sigma'_{\rm HHP}$ to E here has the same sign and density dependence as found by Ramos *et al.*[15] in nuclear matter. The E' in Fig. 13 is essentially the Brueckner-Hartree-Fock energy.

In Fig. 13, E'_C is E/N calculated retaining the imaginary part of $\varepsilon(k)$ in the iteration and omitting $\Sigma'_{\rm HHP}$. A typical imaginary part to $\varepsilon(k)$ is shown in Fig. 4. By comparing E'_C and E'_R, we see that including the imaginary part leads to a somewhat lower E/N. However, the difference is small. This means that the real parts of $\varepsilon(k)$ obtained by iterating with and without $\Sigma''(k)$ are also similar.

We obtained the highest E by iterating with real $\varepsilon(k)$ and including $\Sigma'_{\rm HHP}$ and the lowest E (E'_C) iterating with complex $\varepsilon(k)$ and omitting $\Sigma'_{\rm HHP}$. These ground-state energies E and E'_C represent the maximum "spread" in energy obtained using the present basic method. E and E'_C are shown in Fig. 14 for $D_1^\downarrow$ and $D_3^\downarrow$. We could not use a complex $\varepsilon(k)$ in $\Sigma'_{\rm HHP}$ since the cutoff in y at 2μ and at low y which we used are only valid for real $\varepsilon(k)$.

The full GFHF energy is compared with Monte Carlo values by Panoff and Clark[35] in Fig. 15. The MC values may be regarded as "benchmark" values. From Fig. 15 we see that the GFHF predicts an E which is too high for $D_1^\downarrow$ but too low for $D_3^\downarrow$. This is similar to liquid ^{3}He in which E'_C was comparable but higher than MC values for spin-polarized ^{3}He (Ref. 43) but E'_C lay below the observed E in normal ^{3}He (Ref. 46).

We fitted the polynomial

$$\frac{E}{N}=E_s+Ax^2+Bx^3+Cx^4\ , \tag{31}$$

where $x=(n-n_s)/n_s$ to the GFHF ground-state energies shown in Fig. 15. The resulting saturation energy E_s and density n_s and parameters A, B, and C are listed in Table II. The values of k_F and ε_F^0 at the saturation density n_s are listed in Table III. The value of the Fermi energy

$$\varepsilon_F^0=(\hbar^2/2m)(6\pi^2 n)^{2/3}/N_s^{2/3}$$

depends on the number of spin states N_s. The zero-order kinetic energy $\langle E\rangle=3\varepsilon_F^0/5$ is largest in $D_1^\downarrow$ and smallest in $D_3^\downarrow$ and this sets the relative values of E for $D_1^\downarrow$, $D_2^\downarrow$, and $D_3^\downarrow$. The spin-symmetric interaction Γ^s for $D_1^\downarrow$ contains only odd-angular-momentum components. Particularly, the repulsive s-wave component is excluded. Thus, the potential energy is most attractive in $D_1^\downarrow$ which brings the total energy at saturation E_s of D_1, D_2, and D_3 much closer together than suggested by the kinetic energy alone (see Table III). There is clearly a very sensitive cancellation between kinetic and potential energies making a precise calculation of E difficult.

We included the Cx^4 term in (31) solely to test the sensitivity of n_s, E_s, and A to the fit used. Table II shows that E_s and A are not very sensitive to whether Cx^4 is included in the fit or not, except for A in $D_1^\downarrow$. The compressibility $\kappa^{-1}\equiv V(\partial^2 E/\partial V^2)$ at saturation is

$$(n\kappa)^{-1}=n^2\left[\frac{\partial^2(E/N)}{\partial n^2}\right]_{n=n_s}=2A\ . \tag{32}$$

The value of the compressibility is well determined for $D_2^\downarrow$ and $D_3^\downarrow$ but may be off by 50% in $D_1^\downarrow$.

D. Interaction and Landau parameters

Following Baym and Kadanoff,[18] the interaction appearing in the dynamic susceptibility which is consistent with the self-energy is

$$I_{1212}(12,12)=i\frac{\delta\Sigma_1(1)}{\delta G_2(2)}\ . \tag{33}$$

Using the GFHF self-energy (2), this interaction is, generalized to nondiagonal form,

TABLE III. Saturation properties of $D_1^\downarrow$, $D_2^\downarrow$, and $D_3^\downarrow$ in the GFHF approximation.

	$10^3 n_s$ (Å^{-3})	$n_s\sigma^3$	V_s (cm^3/mol)	k_F (Å^{-1})	ε_F^0 (K)	E_s (K)
$D_1^\downarrow$	3.35	0.163	185	0.578	4.05	0.41
$D_2^\downarrow$	3.17	0.154	196	0.450	2.45	0.029
$D_3^\downarrow$	3.54	0.172	170	0.412	2.02	−0.31

$$I_{1234}(12,34)=\Gamma_{1234}(12,34)+\sum_{5,6}\int d\bar{5}\,\Gamma_{1546}(15,46)G_5(5)G_6(6)\Gamma_{6253}(62,53)\ . \tag{34}$$

The leading term in (34) is the T matrix. The T matrix is the part of the total ph interaction that is primarily responsible for renormalizing the steeply repulsive part of $v(r)$. The second term is called the induced or polarized interaction. It represents the interaction between a ph pair via the density (Γ^s) and the spin-density (Γ^a) excitations. The Landau parameters can be calculated from the proper spin combinations of $I(12,34)$.[47] The Landau limit is most easily understood by defining an alternate set of four-momenta:

$$\begin{aligned} 1&=p+Q\ ,\\ 2&=p'\ ,\\ 3&=p\ ,\\ 4&=p'+Q\ , \end{aligned} \tag{35}$$

where momentum and energy conservation has allowed the number of independent four-vectors to be reduced by one. Physically, Q corresponds to the four-momentum carried through $I(p+Q,p',p,p'+Q)$. The Landau theory refers to the limit $\mathbf{Q}\to 0$ and $|\mathbf{p}|=|\mathbf{p}'|=k_F$. Defining the Landau angle θ_L as the angle subtending $\mathbf{p}$ and $\mathbf{p}'$, reduces $I(p,p',p,p')$ to $I(\cos\theta_L)$. The well-known relation[1] which expresses $I(p,p',p,p')$ in terms of the Fermi-liquid quasiparticle interaction $f(p,p',p,p')$ (and, consequently, the Landau parameters) is

$$f(p,p',p,p')=I(p,p',p,p')+i\int d\bar{q}\,I(p,q,p,q)G^2(q)f(q,p',q,p')\ . \tag{36}$$

We now consider various approximations to this expression. As a first approximation we take

$$f(p,p',p,p')\approx I(p,p',p,p')\approx\Gamma(p,p',p,p')\ .$$

Note that, if $I(p,p',p,p')$ were frequency independent,

$$f(p,p',p,p')\equiv I(p,p',p,p')$$

due to the analytic structure of $G^2(q)$. In Table IV we show Landau parameters calculated from this approximation. The details of the analysis are given by Clements *et al.*[47] and here we mention only that the total energy in the T matrix is set at $E=2\varepsilon(k_F)$. These are Landau parameters at saturation density n_s using the self-consistent T matrix. They are in dimensionless units

$$F_L=\left[\frac{dn}{d\varepsilon}\right]_{\varepsilon_F}f_L=\left[\frac{3\varepsilon_F}{2}\right]nf_L\ , \tag{37}$$

where $(dn/d\varepsilon)_{\varepsilon_F}$ is the density of states per unit volume at ε_F and L denotes the Lth Legendre coefficient. We note firstly that F_0^s is negative. The compressibility κ in Landau theory is given by

$$n\kappa=\frac{1}{n}\left[\frac{dn}{d\varepsilon}\right]_{\varepsilon_F}\frac{1}{1+F_0^s}\ . \tag{38}$$

In order to have a positive compressibility, we must have $F_0^s>-1$. The negative values of F_0^s tell us that the approximations

$$f(p,p',p,p')\approx I(p,p',p,p')\approx\Gamma(p,p',p,p')$$

predict an unstable fluid. It does not properly describe the Landau limit.

Dickhoff *et al.*[48] have shown that the effect of the second term of (36) can be reasonably simulated by replacing the $2\varepsilon(k_F)$ used above by a "starting energy" $E_0(Q)$ given by

$$E_0(Q)=2\int\frac{d^3p}{(2\pi)^3}\frac{n(\mathbf{p})\varepsilon(\mathbf{p})}{\varepsilon(\mathbf{p})-\varepsilon(\mathbf{p}-\mathbf{Q})}\Big/\int\frac{d^3p}{(2\pi)^3}\frac{n(\mathbf{p})}{\varepsilon(\mathbf{p})-\varepsilon(\mathbf{p}-\mathbf{Q})}\ . \tag{39}$$

In the Landau limit, E_0 reduces to $2\varepsilon(k_F)-\frac{4}{3}\varepsilon_F$ where $\varepsilon_F^*=\hbar^2k_f^2/2m^*$ with m^* given by Eq. (29). Our second approximation is then,

$$f(p,p',p,p')\approx I(p,p',p,p')\approx\Gamma(p,p',p,p')$$

but with the energy set equal to E_0 rather than $2\varepsilon(k_F)$. For comparison, the results for the first two approximations are shown in Table V. Similar to the findings of Dickhoff, we find that the starting energy has a

TABLE IV. Landau parameters calculated from the T matrix with starting pair energy $E=2\varepsilon_F$ at saturation in $D_1^\downarrow$, $D_2^\downarrow$, and $D_3^\downarrow$.

	F_0^s	F_1^s	F_2^s	F_3^s	F_4^s	m^*/m
D_1	−1.37	−0.17	0.81	0.70	0.10	0.94
D_2	−4.19	2.01	0.45	0.64	0.31	1.67
D_3	−8.44	4.30	1.10	0.54	0.77	2.43
	F_0^a	F_1^a	F_2^a	F_3^a	F_4^a	
D_2	−0.70	0.01	1.08	0.52	0.11	
D_3	−0.75	0.31	1.01	0.37	0.37	

TABLE V. F_0^s and m^* calculated from the T matrix and from the total $I_{ph}=I_D+I_{\text{ind}}$ for the initial pair energies indicated and from the compressibility via Eqs. (32) and (40).

Method	$D_1^\downarrow$	$D_2^\downarrow$	$D_3^\downarrow$
		F_0^s	
T matrix ($E=2\varepsilon_F$)	−1.4	−4.2	−8.4
T matrix [$E=E_0(Q)$]	−0.58	−1.86	−3.74
T matrix [$E=E_0(Q)$] plus induced with term of Eq. (34)	−0.15	0.18	−1.74
Compressibility, Eq. (40)	0.1±0.4	0.6±0.2	2.3±0.2
		m^*	
T matrix ($E=2\varepsilon_F$)	0.94	1.67	2.43
T matrix ($E=E_0$) plus induced terms	0.89	1.75	2.55

significant influence on the F_0^s. Although the starting energy could also influence F_1^s, we have not performed this calculation. Rather, we note that, in the calculations of Dickhoff, the starting energy has little effect on the F_1^s. Consequently, the effective mass used to calculate the density of states as in (37) were those given by F_1^s listed in Table I.

Finally, the F_0^s calculated from $I(p,p',p,p')$ by adding the induced terms in (34) are also listed in Table V. These values correspond to

$$f(p,p',p,p')\approx\Gamma(p,p',p,p')+I_{\text{ind}}(p,p',p,p') ,$$

where $\Gamma(p,p',p,p')$ is calculated using the starting energy. The details of evaluating I_{ind} can be found in Ref. 47.

The induced interaction contributes a small but non-negligible amount to the total F_1^s. The m^* calculated from the total F_1^s is also listed in Table V. The Landau parameters calculated, with I_{ind} included, use this value for m^* in the density of states. It is immediately apparent from the F_0^s that I_{ind} contributions are substantial. Furthermore, they are more important for $D_2^\downarrow$ and $D_3^\downarrow$ than in $D_1^\downarrow$. This is similar to liquid ^{3}He in which F_0^s, calculated by the first approximation discussed above, is large and negative (−10) for normal ^{3}He but small (−1) for spin-polarized ^{3}He.

F_0^s may be calculated from our calculated values of compressibility (32) by equating (32) and (38). This gives

$$F_0^s=3\frac{A}{\varepsilon_F}-1 . \tag{40}$$

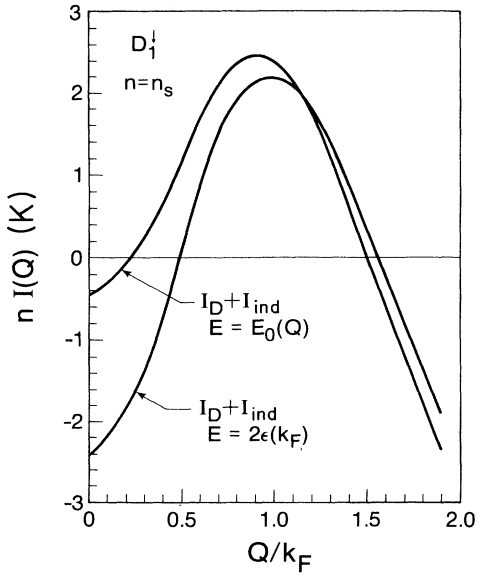

FIG. 16. The particle-hole interaction appearing in the dynamic susceptibility, Eq. (34), (I_D+I_{ind}) for $D_1^\downarrow$ at saturation density $n=n_s$. I_D+I_{ind} for two starting energies in the T matrix are shown.

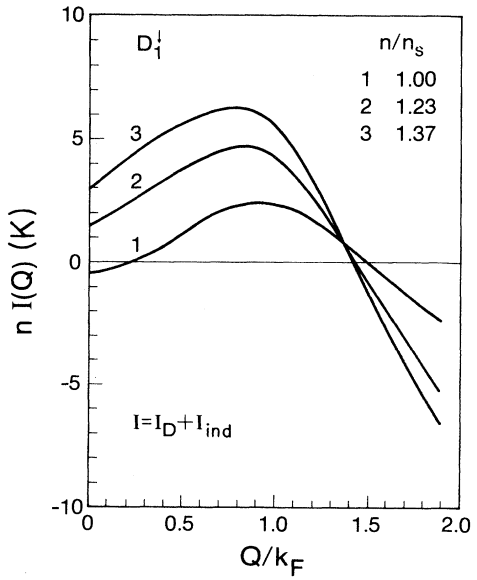

FIG. 17. The density dependence of the interaction $I=I_D+I_{\text{ind}}$ [calculated with $E_0(Q)$] for $D_1^\downarrow$.

These values of F_0^s, often said to include "rearrangement" terms, are higher-order values and are listed in Table V. They are indeed positive and will be more reliable. Comparing these values of F_0^s to those calculated from the different approximations discussed above leads one to conclude that consistency is possible. However, both an accurate calculation of $I(p,p',p,p')$ which includes induced terms and a proper solution of (35) is necessary.

In Fig. 16, we show the real part of $I(Q)$ in $D_1^\downarrow$. The two curves correspond to $I=I_D+I_{\rm ind}$ given by (34) where I_D is the leading term Γ. The $I(Q)$ is a generalization of I from $Q=0$ to finite Q as discussed in Ref. 47. From Fig. 16 we see that the starting energy $E_0(Q)$ adds a positive contribution to I for $Q<k_F$. For still larger Q, the E_0 has little effect. In Fig. 17, the density dependence of $I(Q)$ is displayed. From Fig. 17, we see that $I(Q)$ increases with increasing density.

VI. DISCUSSION

In Fig. 15 we compared the present GFHF ground-state energies with the MC values of Panoff and Clark.[35] For $D_1^\downarrow$ the GFHF E/N lies approximately 0.2 K above the MC value. In nuclear spin-polarized ^{3}He$^\uparrow$, we found[43] the GFHF E/N also lies somewhat above the MC value. However, from Fig. 15 we see that the GFHF E/N for $D_2^\downarrow$ and $D_3^\downarrow$ lies approximately 0.15 K above and below the MC values, respectively. In normal ^{3}He, we found[47] the GFHF energy lies approximately 1 K below the observed value. For more than one spin state (i.e., $D_2^\downarrow$ and $D_3^\downarrow$), the GFHF energy appears to be in error by typically 0.2 K in $D^\downarrow$ with no systematic deviation in sign. The E/N calculated using the correlated basis function method deviates from the MC values by similar amounts but generally in a more systematic way.[34,35] Thus in $D^\downarrow$, the GFHF approximation provides reasonable values of E/N and n_s, but is not as reliable as the CBF method.

The Hugenholtz–van Hove theorem states that the single-particle energy at the Fermi surface $\varepsilon(k_F)$ should equal the energy per particle E/N at zero pressure ($n=n_s$). In Table VI we compare $\varepsilon(k_F)$ and E/N for $D_1^\downarrow$, $D_2^\downarrow$, and $D_3^\downarrow$ calculated in the GFHF approximation. In each case, $\varepsilon(k_F)$ lies approximately 0.3 K below E/N. Thus, we may expect errors in $\varepsilon(k)$ and E/N of approximately this magnitude. This discrepancy reflects the lack of consistency between the $\varepsilon(k)$ and E/N, suggesting particularly that higher-order terms contributing approximately ± 0.3 K remain to be included in the theory.

In Fig. 7 we saw that, for $k\approx k_F$, $\Sigma'_{\rm PPH}(k,\varepsilon_k)$ was typically -4 K and approximately five times as large as $\Sigma'_{\rm HHP}(k,\varepsilon_k)$. Thus, the Brueckner-Hartree-Fock term $\Sigma'_{\rm PPH}$ dominates the self-energy. However, on the level of precision needed to fulfill the Hugenholtz–van Hove theorem, $\Sigma'_{\rm HHP}$ is an important contribution. We note too that the $\Sigma'_{\rm HHP}$ calculated here from (18) differs somewhat from the $\tilde{\Sigma}'_{\rm HHP}$ in (15). The $\tilde{\Sigma}'_{\rm HHP}$ in (15) contains a factor $(1-n_2)$ which requires $\varepsilon_2>\varepsilon_F$. The $\tilde{\Sigma}'_{\rm HHP}$ is strictly the hole-hole-particle $(1-n_2)$ term. The $\tilde{\Sigma}'_{\rm HHP}$ was evaluated by Ramos *et al.*[14,15] and is positive for all k values. The present $\Sigma'_{\rm HHP}$ is negative at small enough k because ε_2 can be far below ε_F in (18) making $\omega_1+\varepsilon_2<y$ possible in (18). We chose to evaluate $\Sigma'_{\rm HHP}$ since this was the term omitted from previous calculations.[33,43] Also, since $\Sigma'_{\rm HHP}$ takes both positive and negative values, its contribution to the total energy E is smaller than that of $\tilde{\Sigma}'_{\rm HHP}$. In previous work we included both $\Sigma''_{\rm PPH}$ and $\Sigma''_{\rm HHP}$.

Perhaps the most interesting result of this work is the enhancement of the effective mass at k_F and its clear relation to spin fluctuations shown in Figs. 9–12. In $D_1^\downarrow$, where the nuclear spins are aligned and spin fluctuations are frozen out, there is no enhancement of $m^*(k)$. In $D_1^\downarrow$ we find $m^*(k_F)\approx 0.90$ in agreement with previous results[33] and with $m^*(k_F)=0.87$ predicted by Dave *et al.*[49] using the correlated random-phase approximation (RPA). In $D_2^\downarrow$ and $D_3^\downarrow$ where spin fluctuations are possible, there is a significant enhancement of $m^*(k)$ at $k\approx k_F$. The enhancement is largest in $D_3^\downarrow$, as seen in Fig. 12. The enhancement arises here principally from $\Sigma'_{\rm HHP}(k,\varepsilon_k)$ which leads to a flattening of $\varepsilon(k,\varepsilon_k)$ at $k\approx k_F$.

The effective mass at the Fermi surface calculated from the Landau parameters $m^*=1+F_1^s/3$ (see Tables I and V) is also consistent with the $m^*(k_F)$ obtained from Fig. 12 in $D_1^\downarrow$, $D_2^\downarrow$, and $D_3^\downarrow$. The Landau parameters F_1^s and m^* change little when the induced term of (34) and the second term in (36) are included (see Table V). In contrast, we found[47] the induced term in (34) enhanced m^* significantly in liquid ^{3}He.

A complex $\varepsilon(k)$ can also be retained in the iterations. This leads to a somewhat lower but comparable ground-state energy. The converged $\varepsilon'(k,\varepsilon_k)$ is also somewhat lower. A complex $\varepsilon(k)$ can also be used to calculate $\Sigma'_{\rm HHP}$, but in this case the cutoff we used is not strictly correct and $\Sigma'_{\rm HHP}$ is overestimated. Using a complex $\varepsilon(k)$ we found an $m^*(k)$ comparable to the results displayed in Figs. 9–12.

Including $\Sigma'_{\rm HHP}$ may be viewed as completing the GFHF approximation. As discussed in Sec. III, the complete GFHF self-energy includes both the first- and second-order self-energy terms with the interaction Γ given by a T matrix. The second-order term, depicted in Fig. 3, may be viewed as the leading term in the "bubble" or RPA series of terms. Blaizot and Friman[50] find that including the whole "bubble" series reduces the size of contributions arising from $\Sigma^{(2)}$ in Fig. 3, at least for a local interaction. It would be interesting to include this "bubble" series using a T matrix to explore its impact in liquid ^{3}He and $D^\downarrow$.

TABLE VI. E/N and single-particle energy at k_F.

	$\varepsilon(k_F)$	E/N
D_1	0.1	0.4
D_2	−0.3	0.0
D_3	−0.6	−0.3

ACKNOWLEDGMENTS

It is a pleasure to thank Dr. Piotr Findiesen for valuable assistance with computations. Support from the U.S. Department of Energy, Office of Basic Energy Sciences, under Contract No. DE-FG02-84ER45082 and from the Natural Science and Engineering Research Council of Canada is gratefully acknowledged.

---

*Present address: Department of Physics, University of Alberta, Edmonton, Alberta, Canada T6G 2J1.

†Present address: Department of Physics, Texas A&M University, College Station, TX 77843-4242.

[1]A. A. Abrikosov, L. P. Gorkov, and I. E. Dzyaloshinski, *Methods of Quantum Field Theory in Statistical Physics* (Prentice-Hall, Englewood Cliffs, New Jersey, 1963).

[2]L. P. Kadanoff and G. Baym, *Quantum Statistical Mechanics* (Benjamin, Menlo Park, 1962).

[3]P. Nozieres, *Theory of Interacting Fermi Systems* (Benjamin, New York, 1964).

[4]A. L. Fetter and J. D. Walecka, *Quantum Theory of Many-Particle Systems* (McGraw-Hill, New York, 1971).

[5]G. E. Brown, *Many-Body Problems* (North-Holland, Amsterdam, 1972).

[6]J. Jeukenne, A. Lejeune, and C. Mahaux, Phys. Rep. C **25**, 83 (1976).

[7]C. Mahaux, P. F. Bortignon, R. A. Broglia, and C. H. Dasso, Phys. Rep. C **120**, 1 (1985).

[8]C. Mahaux and H. Ngo, Nucl. Phys. **A378**, 205 (1982).

[9]V. Bernard and C. Mahaux, Phys. Rev. C **23**, 888 (1981).

[10]R. Sartor and C. Mahaux, Phys. Rev. C **21**, 2613 (1980).

[11]P. Grangé, J. Cugnon, and A. Lejeune, Nucl. Phys. **A473**, 365 (1987).

[12]A. Ramos, W. H. Dickhoff, and A. Polls, Phys. Lett. B **219**, 15 (1989).

[13]W. H. Dickoff, Phys. Lett. B **210**, 15 (1988).

[14]A. Ramos, A. Polls, and W. H. Dickhoff, in *Condensed Matter Theories,* edited by J. S. Arponen, R. F. Bishop, and M. Manninen (Plenum, New York, 1988), Vol. 3, p. 319.

[15]A. Ramos, A. Polls, and W. H. Dickhoff, Nucl. Phys. **A503**, 1 (1989).

[16]M. D. Girardeau, Int. J. Quant. Chem. **17**, 25 (1980).

[17]W. Kolos and L. Wolniewicz, Chem. Phys. Lett. **24**, 457 (1974).

[18]G. Baym and L. P. Kadanoff, Phys. Rev. **124**, 287 (1961).

[19]I. F. Silvera and J. T. M. Walraven, Phys. Rev. Lett. **45**, 1268 (1980); I. Shinkoda, M. W. Reynolds, R. W. Cline, and N. W. Hardy, *ibid.* **57**, 1243 (1986).

[20]R. L. Danilowicz, J. V. Dugan, and R. D. Etters, J. Chem. Phys. **65**, 498 (1976), and earlier references.

[21]W. C. Stwalley and L. H. Nosanow, Phys. Rev. Lett. **36**, 910 (1976); W. C. Stwalley, *ibid.* **37**, 1628 (1976).

[22]L. H. Nosanow, L. J. Parish, and F. J. Pinski, Phys. Rev. B **11**, 191 (1975).

[23]M. D. Miller, L. H. Nosanow, and L. J. Parish, Phys. Rev. Lett. **35**, 581 (1975); Phys. Rev. B **13**, 214 (1976).

[24]M. D. Miller and L. H. Nosanow, Phys. Rev. B **15**, 4376 (1977).

[25]L. H. Nosanow, J. Low Temp. Phys. **23**, 605 (1976); **26**, 613 (1977); J. Phys. (Paris) Colloq. **41**, C7-1 (1980).

[26]E. Krotscheck, R. A. Smith, J. W. Clark, and R. M. Panoff, Phys. Rev. B **24**, 6383 (1981); J. W. Clark, E. Krotscheck, and R. M. Panoff, J. Phys. (Paris) Colloq. **41**, C7-197 (1980).

[27]R. M. Panoff, J. W. Clark, M. A. Lee, K. E. Schmidt, M. H. Kalos, and G. V. Chester, Phys. Rev. Lett. **48**, 1675 (1972).

[28]T. K. Lim, Phys. Rev. B **25**, 2057 (1982).

[29]A. J. Leggett, J. Phys. (Paris) Colloq. **41**, C7-19 (1980).

[30]A. G. K. Modawi, Ph.D. thesis, University of Sussex, 1981.

[31]K. S. Bedell and K. Quader, Phys. Rev. B **31**, 1627 (1984).

[32]S. J. Buckle, J. Phys. C **17**, L633 (1984).

[33]H. R. Glyde and S. I. Hernadi, in *Condensed Matter Theories,* edited by F. B. Malik (Plenum, New York, 1986), Vol. 1.

[34]M. F. Flynn, J. W. Clark, E. Krotscheck, R. A. Smith, and R. M. Panoff, Phys. Rev. B **32**, 2945 (1985).

[35]R. M. Panoff and J. W. Clark, Phys. Rev. B **36**, 5527 (1987).

[36]R. J. Bell, Proc. Phys. Soc. London, Ser. B **7**, 594 (1966).

[37]J. O. Hirschfelder and W. J. Meath, Adv. Chem. Phys. **12**, 3 (1967).

[38]I. F. Silvera, Rev. Mod. Phys. **52**, 393 (1980).

[39]D. G. Friend and R. D. Etters, J. Low Temp. Phys. **39**, 409 (1980).

[40]J. M. V. A. Koelman, H. T. C. Stoaf, B. J. Verhaar, and J. T. M. Walraven, Phys. Rev. Lett. **59**, 676 (1987).

[41]R. M. More, Phys. Rev. Lett. **51**, 396 (1983).

[42]H. R. Glyde and S. I. Hernadi, Phys. Rev. B **29**, 3873 (1984).

[43]R. F. Bishop, M. R. Strayer, and J. M. Irvine, Phys. Rev. B **16**, 3081 (1977).

[44]R. A. Aziz, F. R. W. McCourt, and C. C. K. Wong, Mol. Phys. **61**, 1487 (1987).

[45]G. E. Brown, J. H. Gunn, and P. Gould, Nucl. Phys. **46**, 598 (1963).

[46]H. R. Glyde and S. I. Hernadi, Phys. Rev. B **28**, 141 (1983).

[47]B. E. Clements, C. W. Greeff, and H. R. Glyde (unpublished).

[48]W. H. Dickhoff, A. Faessler, J. Meyer-Ter-Vehn, and H. Müther, Nucl. Phys. **A368**, 445 (1981).

[49]R. D. Dave, J. W. Clark, and R. M. Panoff, Phys. Rev. B **41**, 757 (1990).

[50]J. P. Blaizot and B. L. Friman, Nucl. Phys. **A372**, 69 (1981).